Transitions and the effects of configuration interaction in the spectra of Sn XV–Sn XVIII

R. D'Arcy,[1] H. Ohashi,[2] S. Suda,[2] H. Tanuma,[2] S. Fujioka,[3] H. Nishimura,[3] K. Nishihara,[3] C. Suzuki,[4] T. Kato,[4] F. Koike,[5] J. White,[1] and G. O'Sullivan[1]

[1]*University College Dublin, Belfield, Dublin 4, Ireland*

[2]*Department of Physics, Tokyo Metropolitan University, Hachioji, Tokyo 192-0397, Japan*

[3]*Institute of Laser Engineering, Osaka University, Suita, Osaka 565-0871, Japan*

[4]*National Institute for Fusion Science, Toki, Gifu 509-5292, Japan*

[5]*Physics Laboratory, School of Medicine, Kitasato University, Sagamihara, Kanagawa 228-8555, Japan*

(Received 19 February 2009; published 30 April 2009)

Charge state specific euv spectra from a range of tin ions have been recorded at Tokyo Metropolitan University. The spectra were produced from charge-exchange collisions between tin ions and helium atoms using an electron cyclotron resonance source. At low target gas pressures, the spectra were dominated by single capture events. The spectra were, unexpectedly, found to be dominated by an intense unresolved transition array near 13 nm while the resonance lines, including the previously identified $4p-4d\ ^1S_0\rightarrow{}^1P_1$ resonance line of Sn XV, were relatively weak. From atomic structure calculations, it was found that the unresolved transition array arises from $4s^24p^{m-1}4d-4s^24p^{m-1}4f+4s^24p^{m-2}4d^2$ transitions. In addition it proved necessary to include interaction with core excited $4s4p^m4d$ configurations to fully explain the observed spectra.

DOI: 10.1103/PhysRevA.79.042509 PACS number(s): 32.30.−r

I. INTRODUCTION

In recent years there has been considerable interest in the extreme ultraviolet (euv) spectra of tin ions due to the importance of tin plasmas as potential radiation sources for high intensity operation at $\lambda=13.5$ nm for euv lithography (euvl) [1]. The choice of wavelength is set by the availability of multilayer Mo/Si mirrors that have peak reflectivities of approximately 70% and are efficient reflectors within a 2% bandwidth at this wavelength [2]. The euv spectrum of tin is dominated by an intense unresolved transition array (UTA) overlaid by many strong lines due to $4p^64d^m-4p^54d^{m+1}+4p^64d^{m-2}4f$ transitions in the 13–14 nm region [3], and resonance emission from Sn in stages from eight to thirteen times ionized $1\leq m\leq 6$ lies within the 2% wavelength band. All of the strongest lines from these ion stages have been recently identified in high-resolution vacuum spark spectra by Churilov and Ryabtsev [4,5].

For lower ion stages, $4d-4f$, $4p-4d$, and $4d-5p$ transitions have been identified in Sn VI [6,7], Sn VII [8,9], and Sn VIII [10,11] again from vacuum spark spectra. However in other sources, such as the laser produced or discharge plasmas used in euvl sources, emission from many stages appears at once. Moreover opacity effects, which in an optically thick plasma can dramatically alter the ratio of intensity of high to low oscillator strength lines, make intensity comparisons between theory and experiment extremely difficult. So for these plasmas, unambiguous line identification is almost impossible in the majority of cases especially in regions of high line density, such as the 13–14 nm region where $4p^64d^m-4p^54d^{m+1}+4p^64d^{m-1}4f$ transitions in ion stages from Sn^{8+} to Sn^{13+} overlap significantly in energy. For these spectra, ion separation techniques are an essential prerequisite to any analysis. Such ion stage specific spectra of the emission contributing to the UTA itself have recently been obtained using the charge-exchange method by Tanuma and co-workers [12,13].

Charge exchange spectroscopy has also been used to give ion stage specific spectra of xenon, the other species of interest for euvl, in the euv by Tanuma *et al.* [14] for moderate to highly charged ions and in low charge states, at longer wavelengths with the Uppsala University electron cyclotron resonance (ECR) source [15,16]. Ion stage differentiation is possible in both vacuum spark and charge-exchange spectra since emission from a particular stage may be readily tuned by changing the experimental conditions.

In their earlier work, Tanuma *et al.* [14] reported the observation of spectra from tin in ion stages up to fourteen times ionized. In this work we report on the identification of features in the spectra of fourteen to seventeen times ionized tin and show that configuration-interaction (CI) effects are extremely important in understanding their appearance.

II. EXPERIMENT

Two different methods for production of tin spectra were used. In the first, multiply charged ions were produced in the 14.25 GHz ECR ion source at Tokyo Metropolitan University [14]. A rod of sintered tin oxide was inserted into the plasma chamber and O_2 gas at a pressure of 1×10^{-5} Pa was introduced to produce the plasma and to enhance the population of higher charge states. The multiply charged ions were extracted from the plasma with an electric potential of 20 kV, and charge state specific ions were selected from the ECR source output beam with a 110° double-focusing dipole magnet and allowed to collide with helium atoms at a sufficiently low pressure, ($<10^{-2}$ Pa), such that single collisions and single electron capture were strongly favored. The primary ion beam, which had an approximate diameter of 6 mm, had typically a current in the 0.01–1 μA range. The spectra of ion stage Sn^{q+} result from charge-exchange collisions of Sn^{q+1} ions with helium gas that predominantly cause single electron capture into excited levels of Sn^{q+}.

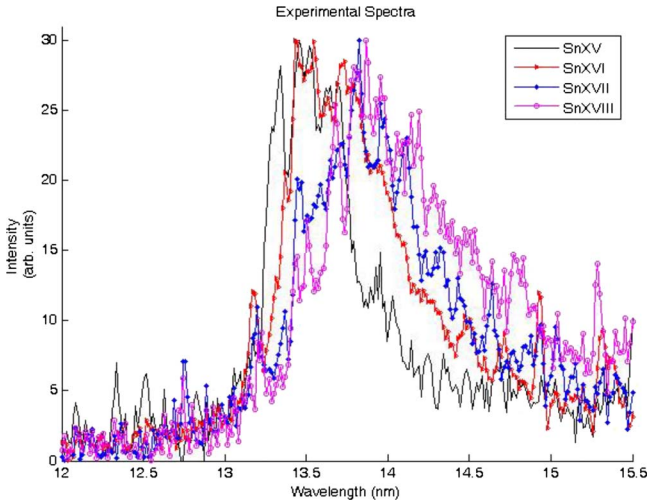

FIG. 1. (Color online) Spectra of Sn ions produced from charge-exchange collisions with He target atoms using ECR source. The spectra of ion Sn^{q+} result from charge-exchange collisions of Sn^{q+1} ions with helium gas that selectively populate certain excited levels of Sn^{q+}.

Spectra were recorded at 90° to the ion-beam direction on a 0.25 m flat field grating spectrograph (SSK-260, Shin Seiki Co.) fitted with an external toroidal mirror to focus the radiation on to a variable line width grating, with approximately 1200 lines mm^{-1} blazed at 100 nm. The detector was a liquid nitrogen cooled charge-coupled device camera (Hamamatsu, 4880) that allowed simultaneous recording over an 18 nm range from 7–25 nm. The slit width was 200 μm which when folded with the pixel width yielded a resolution of 0.03 nm in this wavelength region. O VI and O VII lines arising from O^{6+} and O^{7+} collisions on Xe provided wavelength calibration. The resulting wavelength uncertainty is estimated as 0.02 nm.

In the second set of experiments, the large helical device (LHD) at the National Institute of Fusion Science in Toki was used. The LHD is one of the largest devices in the field of magnetically confined fusion research and plasmas are confined under a magnetic field of 2.75 T at the plasma center.

The typical plasma density is much lower ($\leq 10^{20}$ m^{-3}) than that of laser or discharge produced high-density plasmas (typically $\sim 10^{26}$ m^{-3}), and its spatial profile and electron temperature were measured by a Thomson scattering diagnostic system [17]. Solid tin was introduced by a tracer encapsulated solid pellet (TESPEL) [18] injected into a background hydrogen plasma. The euv spectra were recorded by a grazing incidence spectrometer soft x-ray multichannel spectrometer (SOXMOS) [19] whose groove density and focal length are 600 mm^{-1} and 1 m, respectively. The spectral range was fixed at 11.0–15.2 nm study and the integration time of the detector was typically 200 ms. The overall spectral resolution is about 0.01 nm. The optical axis of the spectrometer was slightly tilted against the equatorial plane within the horizontally elongated plasma cross section because the core temperature tends to be too high to observe euv spectra. The spectrometer was carefully calibrated by observing iron lines that occur as an intrinsic impurity material in the plasma and the absolute wavelength was determined within an accuracy of ± 0.02 nm.

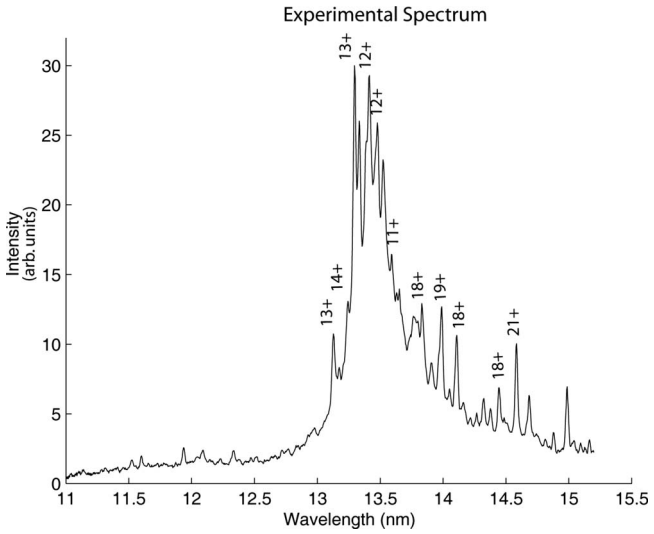

FIG. 2. Spectra of Sn ions from LHD. Emission lines from Sn XII–Sn XXII are present.

III. RESULTS

The spectra obtained at the ECR source are shown in Fig. 1. The spectra of ion Sn^{q+} result from charge-exchange collisions of Sn^{q+1} ions with helium gas. The ion path length through the gas was ~ 1 cm while the mean-free path of the ion was evaluated as 100 cm when the cross section was assumed as 10^{-14} cm^2.

Rather surprisingly, for the most part the spectra are dominated by an intense unresolved transition array in the 13–14 nm region, just like the lower stages. This was completely unexpected since data from experimental data taken from laser produced or discharge produced plasmas of the

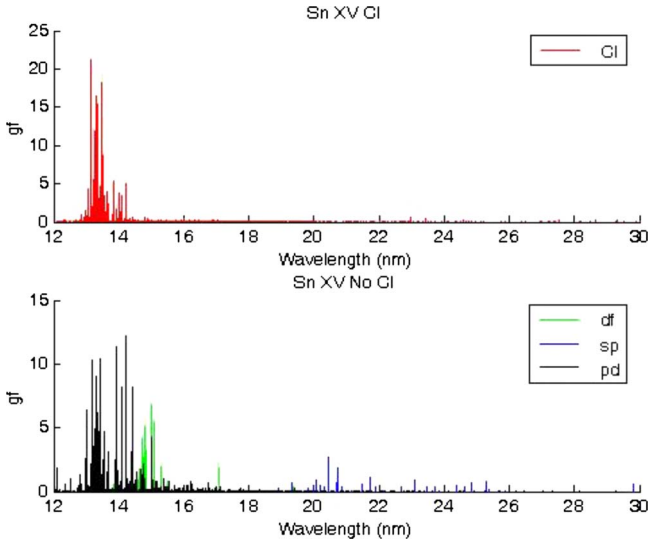

FIG. 3. (Color online) Comparison between CI (top) and non-CI (bottom) calculations for Sn XV.

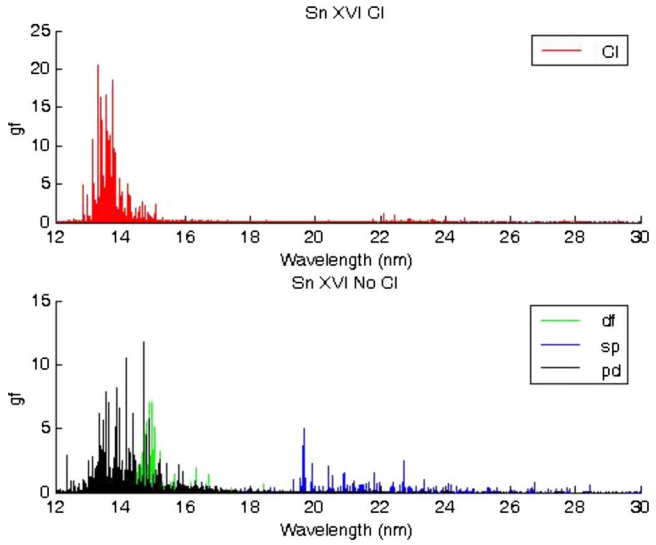

FIG. 4. (Color online) Comparison between CI (top) and non-CI (bottom) calculations for Sn XVI.

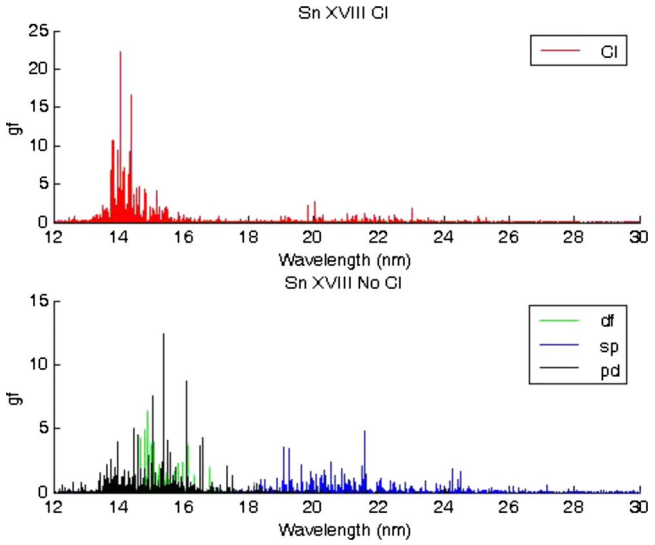

FIG. 6. (Color online) Comparison between CI (top) and non-CI (bottom) calculations for Sn XVIII.

type being considered for euvl all indicate that the in-band emission at 13.5 nm decreases rapidly with increasing plasma temperature (T_e) for values of T_e consistent with production of sizeable populations of open $4p$ subshell ions. Moreover, the spectra were recorded under conditions that only favored single capture events so they cannot be due to open $4d$ shell transitions in lower ion stages. Therefore the data here would indicate that, under certain conditions in which charge transfer is highly favored, intense in-band emission can be sustained for higher plasma electron temperatures than previously considered appropriate.

The ground state of Sn XV is Kr-like $4s^24p^6$ and the resonance $4s^24p^6\ {}^1S_0-4s^24p^54d^1P_1$ transition at 13.2463 nm has been identified by Churilov and Ryabtsev [5]. Although present, it is quite weak in the present spectrum.

In contrast it is clearly seen in Fig. 2, which shows the LHD spectrum. In the LHD study a small amount (0.1% of bulk ion) of tin was introduced into the high-temperature (1000 eV) and low-density ($\sim 10^{19}$ m^{-3}) hydrogen plasma by injecting the TESPEL. The spectrum was measured during a radiative cooling phase 1.5 s after the injection. At this time local electron temperature near the pellet deposition point is around 400 eV. The spectrum is dominated by an intense emission array that contains the strongest $4p^64d^m-4p^54d^{m+1}+4p^64d^{m-2}4f$ lines of Sn VII–XV identified by Churilov and Ryabtsev [4,5]. Apart from the resonance line of Sn XV there is no evidence of the other strong lines seen in the ECR data. However, there is contribution from higher ion stages as the strong lines in the 14–15 nm region arise from stages up to Cu I such as Sn XXII [20]. Thus the CX spectra must arise from the unique excitation mechanism presented by the capture process.

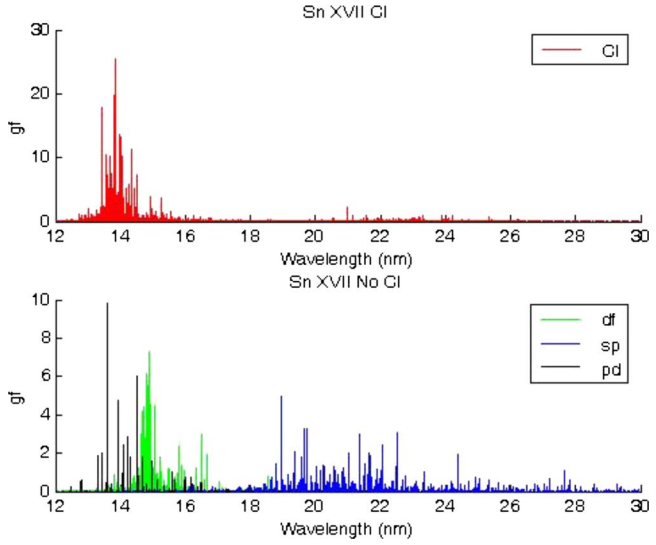

FIG. 5. (Color online) Comparison between CI (top) and non-CI (bottom) calculations for Sn XVII.

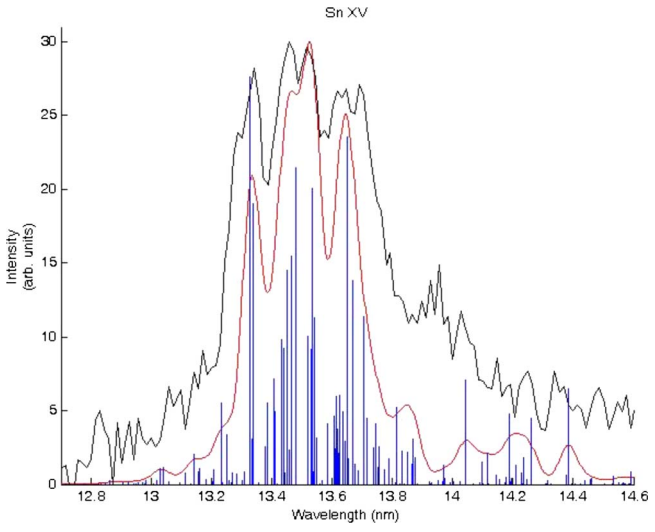

FIG. 7. (Color online) Comparison between a theoretical spectrum for Sn XV convolved with a Gaussian instrumental function and the obtained experimental spectrum of Sn XV. The theoretical data are also presented in the form of stick plots of height equal to the gf value.

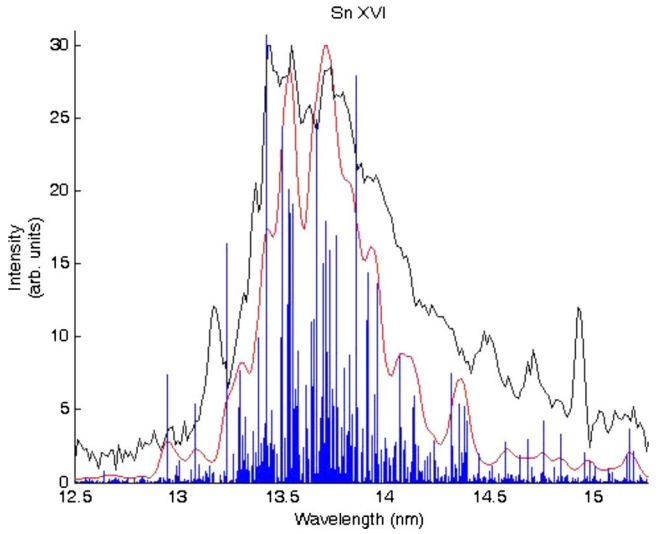

FIG. 8. (Color online) Comparison between a theoretical spectrum for Sn XVI convolved with a Gaussian instrumental function and the obtained experimental spectrum of Sn XVI. The theoretical data are also presented in the form of stick plots of height equal to the gf value.

In order to identify unknown spectral lines, calculations were performed for Sn^{14+}-Sn^{17+} using the Hartree-Fock with Configuration Interaction (HFCI) code of Cowan [21], and while these calculations showed that the only candidate lines at this wavelength should arise from $n=4-n=4$ transitions, the features are too complex in the case of Sn XV and too localized in energy to correspond to resonance $4s^24p^m-4s^24p^{m-1}4d$ lines in the spectra of higher ion stages.

It is well known that spectra obtained in ion-gas collisions often result from the decay of resonantly populated states and the resulting spectra frequently fail to match with intensity predictions calculated *ab initio* without allowance for selective capture processes [22,23]. The energies of the capture states may be estimated from the classical over barrier model [24,25] which in the present case implies capture into states with n significantly greater than 4 so the $n=4$ states must be populated by cascades. For Yrast decays, known to be highly favored in processes involving electron capture [26], population of excited $4f$ states is favored and thus we would expect to observe $4f\rightarrow 4d$ transitions. However a preliminary calculation for $4s^24p^{m-1}4d-4s^24p^{m-1}4f$ failed to reproduce the observed spectra.

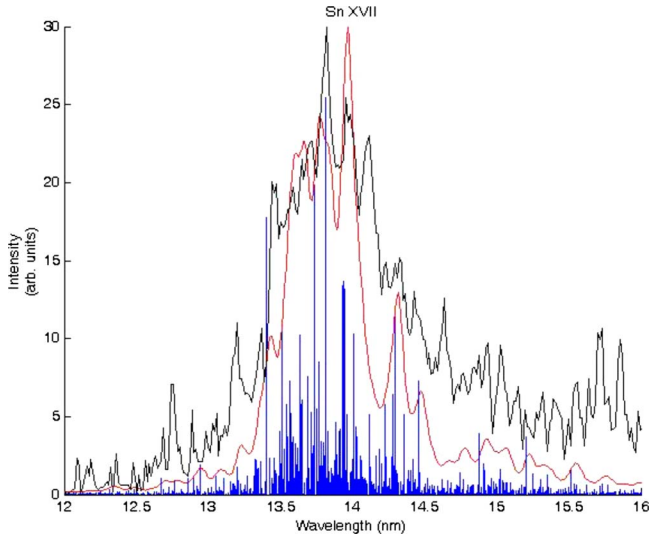

FIG. 9. (Color online) Comparison between a theoretical spectrum for Sn XVII convolved with a Gaussian instrumental function and the obtained experimental spectrum of Sn XVII. The theoretical data are also presented in the form of stick plots of height equal to the gf value.

TABLE I. Calculated and observed energies for the strongest observed lines of the $3d^{10}4s^24p^54d^1\rightarrow 4s^24p^54d^04f^1+4s^24p^44d^2$ transitions of Sn XV.

Transition	λ_{cowan} (nm)	λ_{ECR} (nm)	gf
$^1S_0\rightarrow(4d)^1P_1$	13.25[a]	13.29	5.80
$^3F_4\rightarrow(4f)^3G_5$	13.34	13.34	21.22
$^3D_3\rightarrow(4d)^3F_4$	13.35		14.65
$^3D_2\rightarrow(4d)^1F_3$	13.42	13.46	5.50
$^1D_2\rightarrow(4d)^3F_3$	13.44		7.54
$^3P_2\rightarrow(4d)^3P_2$	13.45		7.08
$^3F_4\rightarrow(4d)^3F_4$	13.46		11.16
$^3D_3\rightarrow(4d)^1F_3$	13.47		11.88
$^1F_3\rightarrow(4f)^1G_4$	13.49		16.54
$^3D_1\rightarrow(4d)^3D_1$	13.53	13.53	5.25
$^3D_2\rightarrow(4d)^3D_2$	13.53		7.74
$^3F_2\rightarrow(4d)^3F_2$	13.54		7.07
$^1F_3\rightarrow(4d)^1F_3$	13.54		8.68
$^3F_3\rightarrow(4f)^3G_4$	13.54		15.43
$^1D_2\rightarrow(4d)^3F_2$	13.55	13.57	6.44
$^3D_2\rightarrow(4d)^3P_1$	13.62	13.62	4.58
$^3P_2\rightarrow(4f)^3F_3$	13.63		4.67
$^1P_1\rightarrow(4d)^1D_2$	13.66	13.65	18.14
$^3F_2\rightarrow(4f)^3G_3$	13.68		10.66
$^3F_4\rightarrow(4d)^3D_2$	13.71	13.70	8.77
$^3D_3\rightarrow(4d)^1D_2$	13.75	13.76	3.18
$^3D_1\rightarrow(4f)^3F_2$	13.82	13.79	4.00
$^3D_2\rightarrow(4f)^3F_3$	14.05	14.03	5.44
$^1F_3\rightarrow(4f)^3F_3$	14.20	14.17	3.71
$^3F_2\rightarrow(4d)^1P_1$	14.27	14.26	3.45
$^1F_3\rightarrow(4d)^3P_2$	14.39	14.36	4.98

[a]The result of the present calculation for the $4p\ ^1S_0-4d\ ^1P_1$ resonance line.

CI effects in spectra where the strongest transitions satisfy $\Delta n=0$ have been shown to be very significant because of the proximity of excitation energies [27,28]. In lower ion stages, when considering transitions from an open $4d$ subshell, excited-state CI of the form $4p^54d^{m+1}+4p^64d^{m-1}4f$ is extremely important and produces a strong spectral narrowing. The effects of CI in the upper-state basis were therefore explored here in some detail. In the present case calculations were performed for excited to excited $4p^{m-1}4d-4p^{m-1}4f+4p^{m-2}4d^2$ transitions $(2\leq m\leq 6)$. Again $4p^{m-1}4f$

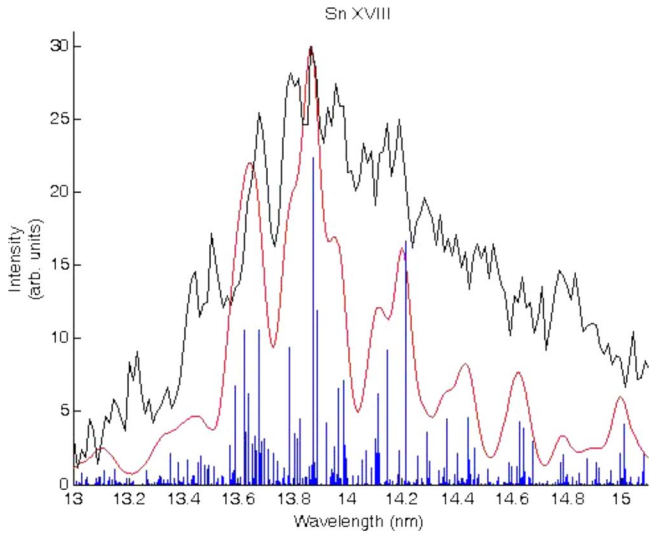

FIG. 10. (Color online) Comparison between a theoretical spectrum for Sn XVIII convolved with a Gaussian instrumental function and the obtained experimental spectrum of Sn XVIII. The theoretical data are also presented in the form of stick plots of height equal to the gf value.

$+4p^{m-2}4d^2$ CI was found to have a dramatic effect on the spectra of each ion stage in going from Sn XV to Sn XVII. Just as in the case of transitions from open $4d$ subshells in lower stages, there is a radical redistribution of oscillator strength accompanied by a strong spectral narrowing and the calculations predict the appearance of a strong line group near 13 nm. However, while this calculation turned out to give good agreement with the observed spectrum for Sn XV, the agreement diminished quite rapidly with increasing ionization and it was necessary to allow for interaction with the lower energy core excited $4s4p^m4d$ configuration in Sn XVI and higher stages.

In Figs. 3–6 we show the results of calculations with and without the inclusion of CI. The transitions considered were $4s^24p^{m-1}4f-4s^24p^{m-1}4d$, $4s^24p^{m-1}4d-4s^24p^{m-2}4d^2$, and $4s^24p^{m-1}4d-4s4p^m4d$. From these calculations it is seen that the CI effects cause a dramatic spectral narrowing, and give an intense feature whose position barely shifts with ion stage and that lies in the original $4p-4d$ excitation region. In particular the effect of CI is to suck up much of the available oscillator strength from longer wavelength $4s^24p^{m-1}4d-4s4p^m4d$ transitions. The results of the CI calculation were then convoluted with a Gaussian of width of 0.03 nm to allow for the effects of instrumental broadening, and the resulting theoretical spectra are shown in Figs. 7–10 together with the underlying line distribution where they are compared to the experimental data. In preparing this figure, the theoretical spectra were shifted by differing amounts to best fit them to the experimental data. Note also that in generating these theoretical spectra the Slater Condon parameters were reduced by 15% while the spin-orbit parameters were left at their *ab initio* values.

A. Spectrum of Sn XV

Here the theoretical spectrum was uniformly shifted through +0.19 eV to obtain optimum agreement between observation and calculation for the strongest lines. From the comparison, it was possible to associate the strong experimental peaks with the strongest predicted lines and these data are given in Table I.

TABLE II. Calculated and observed energies for the strongest observed lines of the $3d^{10}4s^24p^44d^1 \rightarrow 4s^24p^34d^2+4s^24p^44d^04f^1$ transitions of Sn XVI.

Transition	λ_{cowan} (nm)	λ_{ECR} (nm)	gf
$^2S_{1/2} \rightarrow (4d)^2P_{3/2}$	12.95	12.97	4.91
$^2S_{1/2} \rightarrow (4d)^2P_{1/2}$	13.08	13.04	3.59
$^4F_{9/2} \rightarrow (4d)^4G_{11/2}$	13.24	13.19	10.89
$^4F_{7/2} \rightarrow (4d)^2G_{9/2}$	13.30	13.32	5.10
$^2P_{3/2} \rightarrow (4d)^2D_{5/2}$	13.32[a]		8.11
$^2D_{5/2} \rightarrow (4d)^2F_{7/2}$	13.39	13.37	6.62
$^2G_{9/2} \rightarrow (4f)^2H_{11/2}$	13.43	13.43	20.48
$^2F_{7/2} \rightarrow (4d)^2G_{7/2}$	13.49		6.63
$^2F_{7/2} \rightarrow (4d)^2G_{9/2}$	13.50		16.22
$^4F_{9/2} \rightarrow (4d)^2H_{11/2}$	13.53	13.55	8.11
$^4D_{7/2} \rightarrow (4f)^4F_{9/2}$	13.54		13.38
$^2F_{7/2} \rightarrow (4d)^4F_{9/2}$	13.54		12.29
$^2D_{5/2} \rightarrow (4d)^2F_{7/2}$	13.55		12.70
$^4D_{5/2} \rightarrow (4f)^4F_{7/2}$	13.64	13.63	7.06
$^4D_{7/2} \rightarrow (4d)^4D_{7/2}$	13.64		7.33
$^2F_{7/2} \rightarrow (4d)^2F_{7/2}$	13.65		7.46
$^2G_{7/2} \rightarrow (4f)^2H_{9/2}$	13.67	13.73	16.57
$^2G_{9/2} \rightarrow (4d)^2G_{9/2}$	13.70		9.98
$^2D_{5/2} \rightarrow (4d)^2F_{7/2}$	13.71		11.91
$^4F_{9/2} \rightarrow (4d)^4F_{9/2}$	13.73		10.63
$^2P_{3/2} \rightarrow (4f)^2D_{5/2}$	13.77	13.79	11.28
$^4P_{5/2} \rightarrow (4f)^4G_{7/2}$	13.80		5.23
$^2G_{7/2} \rightarrow (4f)^2G_{7/2}$	13.82		5.82
$^2D_{3/2} \rightarrow (4d)^2F_{5/2}$	13.86	13.88	18.55
$^2P_{1/2} \rightarrow (4d)^2D_{3/2}$	13.91	13.93	7.41
$^4F_{7/2} \rightarrow (4f)^2G_{9/2}$	13.92		9.60
$^2D_{5/2} \rightarrow (4f)^2F_{7/2}$	13.96	13.95	9.07
$^2D_{3/2} \rightarrow (4f)^2F_{5/2}$	13.96		8.31
$^2D_{3/2} \rightarrow (4d)^2D_{3/2}$	14.07	14.07	5.74
$^2D_{5/2} \rightarrow (4f)^2F_{7/2}$	14.13	14.11	3.41
$^2D_{5/2} \rightarrow (4d)^2D_{5/2}$	14.14	14.15	3.94
$^2D_{5/2} \rightarrow (4d)^2D_{5/2}$	14.32	14.32	5.00
$^2G_{9/2} \rightarrow (4f)^2G_{9/2}$	14.36	14.36	3.61
$^2D_{3/2} \rightarrow (4d)^2P_{1/2}$	14.38	14.40	3.47

[a]Calculated resonance line.

B. Spectrum of Sn XVI

In this case the theoretical spectrum was uniformly shifted through +0.1 eV to obtain optimum agreement for the strongest lines. From the comparison, it was again possible to associate the strong experimental peaks with the strongest predicted lines and these data are given in Table II. Note that

TABLE III. Calculated and observed energies for the strongest observed lines of the $3d^{10}4s^24p^34d^1 \rightarrow 4s^24p^24d^2+4s^24p^34d^04f^1$ transitions of Sn XVII.

Transition	λ_{cowan} (nm)	λ_{ECR} (nm)	gf
$^3P_2 \rightarrow (4d)^3D_3$	13.37[a]	13.37	8.91
$^3G_5 \rightarrow (4f)^3H_6$	13.40	13.43	17.79
$^1D_2 \rightarrow (4d)^1F_3$	13.46[a]	13.47	10.82
$^1G_4 \rightarrow (4d)^3G_5$	13.51	13.50	10.47
$^3F_4 \rightarrow (4d)^1H_5$	13.54	13.55	5.78
$^3P_0 \rightarrow (4d)^3D_1$	13.55		3.69
$^3G_4 \rightarrow (4f)^3G_5$	13.57		7.26
$^5D_3 \rightarrow (4d)^5P_3$	13.58	13.59	5.17
$^3P_2 \rightarrow (4f)^3D_3$	13.59		3.72
$^5D_4 \rightarrow (4f)^5F_5$	13.64	13.65	10.25
$^3F_4 \rightarrow (4d)^3F_4$	13.65		6.05
$^5D_4 \rightarrow (4d)^5D_4$	13.69	13.72	7.58
$^3D_3 \rightarrow (4d)^3F_4$	13.74		19.81
$^1F_3 \rightarrow (4d)^1G_4$	13.82	13.82	25.43
$^3D_1 \rightarrow (4f)^3F_2$	13.93	13.95	13.41
$^3F_4 \rightarrow (4f)^3G_5$	13.94		13.70
$^1D_2 \rightarrow (4f)^1F_3$	13.95		13.20
$^3P_2 \rightarrow (4f)^3D_3$	14.00	13.99	10.32
$^1D_2 \rightarrow (4d)^1D_2$	14.23	14.23	5.74
$^1P_1 \rightarrow (4f)^1D_2$	14.29	14.29	11.35
$^1F_3 \rightarrow (4d)^1F_3$	14.46	14.43	7.25

[a]Calculated resonances lines.

in this spectrum, when the calculations were restricted to only allow for $4p^44f+4p^34d^2$ CI rather than $4s^24p^44f+4s^24p^34d^2+4s4p^54d$, the agreement for the transitions on the low energy side of the UTA was not as good, and in particular the lines responsible for experimental peaks observed at 13.73 and 13.79 nm were shifted to 14 nm and beyond so that the theoretical spectrum essentially appeared to reverse the intensities of the line groups observed near 13.73 and 13.95, and shift them to lower energy. The lines identified from the full CI calculation are presented in Table II together with their calculated oscillator strengths. Once again all of the most intense lines with gf values of five or greater in the UTA region are accounted for.

C. Spectrum of Sn XVII

For Sn^{16+} the theoretical spectrum was uniformly shifted through −0.05 eV to obtain optimum agreement between observation and calculation for the strongest lines. From the comparison, it was again possible to associate the strong experimental peaks within the UTA (13–14.5 nm region) with the strongest predicted lines and these data are given in Table III. In addition in this spectrum a number of strong lines appear in the 14.5–16 nm region. While their origin is unclear, they do not appear to arise from $n=4-n=4$ transitions nor do they arise from $\Delta n \geq 1$ transitions involving the $n=4$ shell as lines from these are expected at much higher photon energy.

TABLE IV. Calculated and observed energies for the strongest observed lines of the $3d^{10}4s^24p^24d^1 \rightarrow 4s^24p^14d^2+4s^24p^24d^04f^1$ transitions of Sn XVIII.

Transition	λ_{cowan} (nm)	λ_{ECR} (nm)	gf
$^2D_{5/2} \rightarrow (4d)^2F_{7/2}$	13.44[a]	13.44	10.14
$^4P_{5/2} \rightarrow (4f)^4D_{7/2}$	13.59	13.51	6.78
$^4F_{9/2} \rightarrow (4f)^4G_{11/2}$	13.62	13.68	10.59
$^2D_{3/2} \rightarrow (4d)^2F_{5/2}$	13.64		6.19
$^2F_{5/2} \rightarrow (4d)^2F_{7/2}$	13.68		10.58
$^2D_{3/2} \rightarrow (4d)^2F_{5/2}$	13.77[a]	13.78	5.30
$^2D_{5/2} \rightarrow (4f)^2F_{7/2}$	13.79	13.81	9.42
$^4P_{3/2} \rightarrow (4d)^4D_{5/2}$	13.79		5.49
$^2F_{7/2} \rightarrow (4d)^2G_{9/2}$	13.87	13.87	22.34
$^2F_{7/2} \rightarrow (4d)^2G_{9/2}$	13.87		6.75
$^2G_{9/2} \rightarrow (4f)^2H_{11/2}$	13.89		11.92
$^2F_{5/2} \rightarrow (4f)^2G_{7/2}$	13.97	13.95	6.53
$^2F_{7/2} \rightarrow (4f)^2H_{9/2}$	13.99		7.12
$^2G_{7/2} \rightarrow (4d)^4F_{9/2}$	14.11	14.09	6.20
$^2D_{3/2} \rightarrow (4f)^2F_{5/2}$	14.15	14.15	9.20
$^2D_{5/2} \rightarrow (4d)^2G_{7/2}$	14.21	14.19	16.62
$^2P_{3/2} \rightarrow (4d)^2D_{5/2}$	14.21		7.07

[a]Calculated resonances lines.

D. Spectrum of Sn XVIII

Here the theoretical spectrum was uniformly shifted through −0.18 eV. Again, from the comparison, it was possible to associate the strong experimental peaks with the strongest predicted lines within the UTA or in the 13–14.5 nm region, and these data are given in Table IV. In this spectrum the longer wavelength lines are much more pronounced pointing to the fact that another strong transition group is overtaking the $4s^24p^24d-4s^24p^24f+4s^24p4d^2+4s4p^34d$ in importance for the conditions of the present experiment. We are currently trying to identify the transitions responsible for these lines.

IV. CONCLUSION

We have succeeded in identifying the strongest lines arising from $4s^24p^{m-1}4d-4s^24p^{m-1}4f+4s^24p^{m-2}4d^2$ transitions in Sn XV–Sn XVIII. It was found that, in interpreting this spectrum, it was necessary to allow for $4p^{m-1}4f+4p^{m-2}4d^2+4s4p^m4d$ CI. Such interactions, already known to dominate open $4d$ subshell spectra appear to be a universal feature associated with $\Delta n=0,4-4$ excitation. Moreover, the fact that these transitions dominate the spectra and are seen to make a strong contribution in the wavelength range required for euvl show that a novel source arrangement based on a forced recombination scheme, in which electrons from a surrounding plasma are captured by tin ions in stages from Sn^{15+}-Sn^{18+}, might provide an interesting addition to existing sources. Such a scheme has already been shown to significantly increase the efficiency of H-like Li emission at 13.5

nm [29,30]. In the present case, since the transitions are between excited states the problem of self-absorption that has been shown to be the major limiting factor on euv conversion efficiency does not arise and provides an added attraction for such a forced recombination scheme.

ACKNOWLEDGMENTS

This work was partly supported by the research collaboration program in NIFS. One of the authors (G.O.S.) wishes to acknowledge MEXT leading project on euv sources in Osaka University and SFI STTF.

[1] G. O'Sullivan, A. Cummings, P. Dunne, P. Hayden, L. McKinney, N. Murphy, and J. White, *EUV Sources for Lithography*, edited by Vivek Bakshi (SPIE, Bellingham, WA, 2006), Chap. 5.
[2] D. T. Attwood, *Soft X-rays and Extreme Ultraviolet Radiation: Principles and Applications* (Cambridge University Press, Cambridge, 2000).
[3] G. D. O'Sullivan and R. Faulkner, Opt. Eng. **33**, 3978 (1994).
[4] S. S. Churilov and A. N. Ryabtsev, Phys. Scr. **73**, 614 (2006).
[5] S. S. Churilov and A. N. Ryabtsev, Opt. Spectrosc. **660**, 729 (2006).
[6] Y. N. Joshi and A. M. van Kleef Th, Can. J. Phys. **55**, 714 (1977).
[7] S. S. Churilov, R. R. Kildyarova, A. N. Ryabtsev, A. E. Kramida, and Y. N. Joshi, Phys. Scr. **50**, 463 (1994).
[8] Y. N. Joshi and G. J. van het Hof, Phys. Scr. **48**, 719 (1993).
[9] V. I. Azarov, Y. N. Joshi, S. S. Churilov, and A. N. Ryabtsev, Phys. Scr. **50**, 642 (1994).
[10] V. I. Azarov and Y. N. Joshi, J. Phys. B **26**, 3495 (1993).
[11] S. S. Churilov and A. N. Ryabysev, Opt. Spectrosc., **100**, 660 (2006).
[12] H. Tanuma, H. Ohashi, S. Fujioka, H. Nishimura, A. Sasaki, and K. Nishihara, J. Phys.: Conf. Ser. **58**, 231 (2007).
[13] K. Nishihara, A. Sunahara, A. Sasaki, M. Numami, H. Tanuma, S. Fujioka, Y. Shimada, K. Fujima, H. Furukawa, T. Kato, F. Koike, R. More, M. Murakami, T. Nishikawa, V. Zhakhovskii, K. Gamata, A. Takata, H. Ueda, H. Nishimura, Y. Izawa, N. Miyanaga, and K. Mima, Phys. Plasmas **15**, 056708 (2008).
[14] H. Tanuma, H. Ohashi, E. Shibuya, N. Kobayashi, T. Okuno, S. Fujioka, H. Nishimura, and K. Nishihara, Nucl. Instrum. Methods Phys. Res. B **235**, 331 (2005).
[15] M. Larsson, A. Gonzales, R. Hallin, F. Heijkenskjöld, R. Hutton, A. Langereis, B. Nystrom, G. O'Sullivan, and A. A. Wännström, Phys. Scr. **51**, 69 (1995).
[16] M. Larsson, A. Gonzales, R. Hallin, F. Heijkenskjöld, B. Nystrom, G. O'Sullivan, C. Weber, and A. A. Wännström, Phys. Scr. **53**, 317 (1996).
[17] K. Narihara, I. Yamada, H. Hayashi, and K. Yamauchi, Rev. Sci. Instrum. **72**, 1122 (2001).
[18] S. Sudo, J. Plasma Fusion Res. **69**, 1349 (1993).
[19] J. L. Schwob, A. W. Wouters, and S. Suckewer, Rev. Sci. Instrum. **58**, 1601 (1987).
[20] C. Suzuki, T. Kato, K. Sato, N. Tamura, D. Kato, S. Sudo, N. Yamamoto, H. Tanuma, H. Ohashi, S. Suda, G. O'Sullivan, and A. Sasaki, IOP Conf. Ser. (to be published).
[21] R. D. Cowan, *The Theory of Atomic Structure and Spectra* (University of California Press, Berkeley, 1991).
[22] J. Burgdörfer, R. Morgenstern, and A. Niehaus, Nucl. Instrum. Methods Phys. Res. B **23**, 120 (1987).
[23] M. Wang, F. O'Reilly, P. Dunne, A. Arnesen, F. Heijkenskjöld, R. Hallin, and G. O'Sullivan, J. Phys. B **30**, 4175 (1997).
[24] A. Barany *et al.*, Nucl. Instrum. Methods Phys. Res. B **9**, 397 (1985).
[25] A. Niehaus, J. Phys. B **19**, 2925 (1986).
[26] O. Vogel, Phys. Scr. **42**, 341 (1990).
[27] F. Koike, S. Fritzsche, K. Nishihara, A. Sasaki, T. Kagawa, T. Nishikawa, K. Fujima, T. Kawamura, and H. Furukawa, J. Plasma Fusion Res. **7**, 253 (2006).
[28] P. Mandelbaum, M. Finkenthal, J. L. Schwob, and M. Klapisch, Phys. Rev. A **35**, 5051 (1987).
[29] A. Nagano, T. Mochizuki, S. Miyamoto, and S. Amano, Appl. Phys. Lett. **93**, 091502 (2008).
[30] A. Nagano, T. Inoue, P. E. Nica, S. Amano, S. Miyamoto, and T. Mochizuki, Appl. Phys. Lett. **90**, 151502 (2007).